Proudman
Oceanographic
Laboratory

A Third Generation Wave Model of European Continental Shelf Seas

with Depth and Current Refraction due to Tides and Surges and its Validation using GEOSAT and Buoy Measurements

X Wu, R A Flather and J Wolf
Report No 33 1994

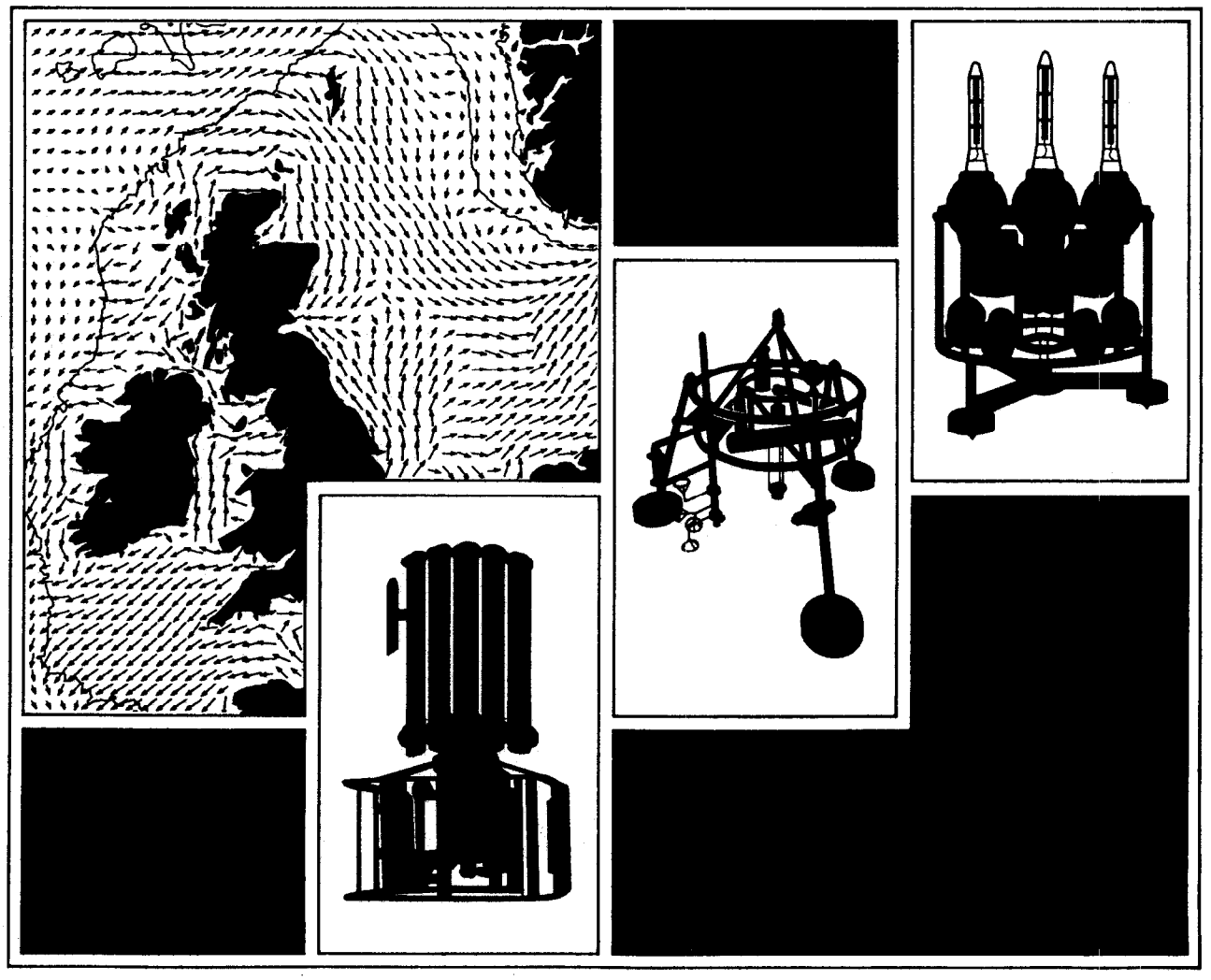

Natural Environment Research Council

PROUDMAN OCEANOGRAPHIC LABORATORY

Bidston Observatory,
Birkenhead, Merseyside, L43 7RA, U.K.

Telephone: 051 653 8633
Telex 628591 OCEANB G
Telefax 051 653 6269

Director: Dr. B.S. McCartney

Natural Environment Research Council

PROUDMAN OCEANOGRAPHIC LABORATORY

REPORT NO. 33

A Third Generation Wave Model of European Continental Shelf Seas With Depth and Current Refraction Due to Tides and Surges and Its Validation Using GEOSAT and Buoy Measurements

Xiaoming Wu, Roger A. Flather & Judith Wolf

1994

DOCUMENT DATA SHEET

AUTHOR	PUBLICATION DATE
Wu, X., Flather, R.A. & Wolf, J.	1994

TITLE: A Third Generation Wave Model of European Continental Shelf Seas With Depth and Current Refraction Due to Tides and Surges and Its Validation Using GEOSAT and Buoy Measurements

REFERENCE: Proudman Oceanographic Laboratory, Report No.33, 48pp.

ABSTRACT

A shallow water third generation wave prediction model coupled with a barotropic tide and surge model is set up for the European continental shelf seas. By including a depth and current refraction scheme, this model takes into account temporally and spatially varying sea surface elevations and depth mean currents due to tide and surge motion. An energy forcing scheme is proposed and applied to the model's open boundaries to account for the propagation of swells into the system. A hindcast study is carried out for the "Great Storm" in October 1987, which is also identified from processing GEOSAT data. Newly developed schemes are applied to further increase the reliability and accuracy of altimeter-derived wave and wind data. Spatial variations of modelled significant wave height (SWH) are examined by comparison with GEOSAT altimeter-derived data, while temporal variations of wave parameters are studied using buoy measurements. The wind fields used to drive the wave model are also compared with measurements to assess the correlation between the accuracy of wave prediction and the quality of wind data. Results demonstrate that the proposed simple open boundary scheme is effective in accounting for the wave energy input at boundaries. Separate depth and current effect may each modulate SWH by up to 0.5m (or 40%, whichever the lower) due to its interaction with waves. Refraction of waves is predominantly caused by changes in water depth in the North Sea and by wave-current interaction in some parts of the Irish Sea, while in the English Channel they appear to be equally important. The refraction effects are more distinct at storm peaks, and improvements in wave hindcast are found at several places. Errors in the wave hindcast appear to be mainly associated with errors in wind field specifications.

ISSUING ORGANISATION	TELEPHONE
Proudman Oceanographic Laboratory Bidston Observatory Birkenhead, Merseyside L43 7RA UK Director: Dr B S McCartney	051 653 8633
	TELEX 628591 OCEAN BG
	TELEFAX 051 653 6269

KEYWORDS		CONTRACT
MATHEMATICAL MODELS WAVES TIDES SURGES GEOSAT	REGION NWEUR CONTINENTAL SHELVES ENGLISH CHANNEL NWEUR CHA NORTH SEA NWEUR NOR IRISH SEA	PROJECT MHT-43-1 PRICE £15

Copies of this report are available from:
The Library, Proudman Oceanographic Laboratory.

CONTENTS Page No.

1. INTRODUCTION

Since the first operational wave prediction scheme developed by Sverdrup and Munk (1947), numerical wave prediction models have gone through three major stages of development, taking place in the 1960's, 70's and 80's, respectively. The state-of-the-art "third generation" wind wave prediction model, developed by the WAM (WAve Modelling) group, has made substantial progress in replacing the paramerization of processes with a full physical description (WAMDI, 1988). More recently, Hubbert and Wolf (1991) incorporated a depth and current refraction scheme into a WAM wave prediction model in order to investigate wave refraction by temporally and spatially varying water depth and current. Studies of a number of idealised cases showed that the effects of depth and current refraction are not limited to just a turning of the waves, but also involve significant changes in the shape of the wave spectra.

In shallow water continental shelf seas, the influence of changes in water levels and currents on wave propagation can be quite significant. Examples of the interaction between waves and tidal currents in the southern North Sea were given by Vincent (1979), who observed a tidal modulation of significant wave height with an amplitude of 0.25m. Clayson and Ewing (1988) also found semi-diurnal tidal current influence on the modulation of measured waves in the North Sea. A pronounced refraction effect of the bottom topography on surface waves was found by Aranuvachapun (1977), who compared wave estimates obtained from a wave refraction diagram method with measurements at some North Sea stations. Storm surges generated in close association with waves modify the total water depth and current. Calculations (Wolf et al. 1988) showed that the refraction of waves by tide and surge currents as well as water depth changes can be significant in shallow water, with long period waves particularly affected. Tolman (1991) found that tides mainly result in oscillations of mean wave parameters, whereas surges result in systematic variations, and due to accumulation of effects small wind-induced currents might have a larger impact on wave parameters than large but oscillating tidal currents. A combined wave and tide/surge model is currently being developed at the Proudman Oceanographic Laboratory (POL). This model takes into account various interaction processes between waves and tides and surges, and is expected to give improved forecasts of waves, sea surface elevations and currents.

In this report a shallow water version of a third generation wave model derived from the WAM model with a depth and current refraction scheme is set up for the NW European continental shelf seas. Unlike some other limited area wave prediction models which use unrealistic closed boundaries uniformly, an energy forcing scheme is applied to the model's open boundaries, in an attempt to simulate the propagation of the North Atlantic swells into the modelled region. Furthermore, this model considers time-varying water depths and currents due to the propagation of tides and surges, by means of a barotropic tide and surge model which is run simultaneously to update total water levels and depth mean currents at regular time intervals.

The wave model is used to hindcast waves during the severe storm of 15-17 October 1987, which was associated with a fast moving intense depression tracking NNE from the Bay of Biscay to the central North Sea. The storm caused extensive damage in the southeast England and at least 17 deaths. A detailed description of the meteorological situation during the passage of the storm across the European coast and some aftermath analyses can be found in the U.K. Met. Office Report (1988). An analysis of the GEOSAT altimeter-derived wind and wave data has been carried for the entire North East Atlantic area. The "Great Storm" of October 1987 is clearly identified in the analyzed data set. This provides an excellent opportunity for the intercomparison of model results with GEOSAT altimeter-derived data in a wide spatial domain, which complements the comparison of model results with in-situ buoy measurements in the time domain at some fixed locations.

Satellite observation has an unique role in providing a wide spatial coverage of sea-state data. Intercomparison studies of satellite data and model results have been previously carried out for validation of wind and wave models (see WAMDI,1988), and for validation and assimilation of satellite data (Janssen et al.1987, Hasselmann et al.1988 and Bauer et al.1992). Using GEOSAT altimeter wave height data, Romeiser (1992) carried out a validation study of the global WAM model by comparing global significant wave height fields for the entire year of 1988. Pronounced differences between the wave heights from GEOSAT and WAM near coasts and in the vicinity of groups of small islands were evident in monthly averaged wave height maps. These were attributed to the coarse spatial resolution (3°x3°) of the model and to the absence of shallow water extensions in the global WAM model used in

the study, as well as to errors in wind stress data. It was also shown that the definition of the southern limit of the WAM model grid as a closed boundary is sometimes inadequate. Guillaume and Mognard (1992) recently proposed new methods for the validation of altimeter-derived sea state parameters with results from wind and wave models. The GEOSAT data set over the North Atlantic was compared with surface winds from the ECMWF (the European Centre for Medium-Range Weather Forecast) model analysis and with significant wave heights (SWH) from METEO FRANCE VAG wave model (a deep water wave model with a resolution of approximately 100km covering the North Atlantic). However, those parts of GEOSAT tracks over the North Sea were discarded, restricting the comparison to the open ocean, away from the boundaries of the VAG model.

This report is organized as follows. In Section 2, we present a shallow water wave model with depth and current refraction, together with an open boundary energy forcing scheme. We also give a description of the coupling of the model with a barotropic tide and surge model and the application of the coupled model to a wave hindcast during the "Great Storm" of October 1987 in the European continental shelf seas. In Section 3, we describe the analysis of GEOSAT wind and wave data sets with some newly developed schemes that are aimed at further increasing the reliability and accuracy of altimeter data. We also describe the in-situ buoy data gathered at three Rijkswaterstaat (RWS) stations and at the Amoco Leman platform. Section 4 is devoted to the intercomparison of observed and modelled wind and wave data in both the spatial and temporal domains. The results are summarized and discussed in Section 5, while Section 6 gives a conclusion on this work and outlook for future studies.

2. THE WAVE MODEL AND HINDCAST STUDY

The wave model solves the wave action balance equation for the directional wave action density spectrum $N(\omega_o,\theta;\underline{x},t)$, which is the conserved quantity in the presence of currents (Bretherton and Garrett,1969) if the source terms are neglected, with ω_o denoting the intrinsic angular frequency, θ the wave direction, $\underline{x}$ the two dimensional spatial coordinates and t the time. Based on the transport equation of wave energy spectrum $E(\omega_o,\theta;\underline{x},t)$ (WAMDI,1988), using the definition $E = \omega_o N$, the wave action density equation is derived as follows (see Hubbert and Wolf,1991)

$$\frac{dN}{dt} + \frac{\partial}{\partial\theta}\left(N\frac{d\theta}{dt}\right) + \frac{\partial}{\partial\omega_o}\left(N\frac{d\omega_o}{dt}\right) = \frac{S}{\omega_o}\,, \tag{1}$$

where, in spherical polar coordinates (latitude ϕ, longitude ψ),

$$\begin{aligned}\frac{dN}{dt} &= \frac{\partial N}{\partial t} + \nabla\cdot(\underline{u}+\underline{c}_g)N \\ &= \frac{\partial N}{\partial t} + \frac{1}{R\cos\phi}\frac{\partial}{\partial\psi}[(u+c_g\sin\theta)N] + \frac{1}{R\cos\phi}\frac{\partial}{\partial\phi}[(v+c_g\cos\theta)N\cos\phi]\,,\end{aligned} \tag{2}$$

$$\begin{aligned}\frac{d\theta}{dt} &= \dot{\theta}_{gc} + \frac{|\underline{k}\times\nabla|D}{k^2}\frac{\partial\omega_o}{\partial D} + \frac{\underline{k}\cdot|\underline{k}\times\nabla|\underline{u}}{k^2} \\ &= \frac{c_g}{R}\sin\theta\tan\phi + \frac{\omega_o}{R\sinh 2kD}\left(\sin\theta\frac{\partial D}{\partial\phi} - \frac{\cos\theta}{\cos\phi}\frac{\partial D}{\partial\psi}\right) \\ &\quad + \frac{\sin\theta}{R}\left(\sin\theta\frac{\partial u}{\partial\phi} + \cos\theta\frac{\partial v}{\partial\phi}\right) - \frac{\cos\theta}{R\cos\phi}\left(\sin\theta\frac{\partial u}{\partial\psi} + \cos\theta\frac{\partial v}{\partial\psi}\right)\,,\end{aligned} \tag{3}$$

$$\frac{d\omega_o}{dt} = -D\nabla\cdot\underline{u}\frac{\partial\omega_o}{\partial D} - \underline{c_g}\cdot(\underline{k}\cdot\nabla)\underline{u}$$

$$= -\frac{\omega_o kD}{R\sinh 2kD}\left(\frac{1}{\cos\phi}\frac{\partial u}{\partial\psi} + \frac{\partial v}{\partial\phi} - v\tan\phi\right) - \frac{c_g k}{R}\cos\theta\left(\sin\theta\frac{\partial u}{\partial\phi} + \cos\theta\frac{\partial v}{\partial\phi}\right) \qquad (4)$$

$$- \frac{c_g k}{R}\left[\frac{\sin\theta}{\cos\phi}\left(\sin\theta\frac{\partial u}{\partial\psi} + \cos\theta\frac{\partial v}{\partial\psi}\right) - \cos\theta\tan\phi(u\sin\theta + v\cos\theta)\right],$$

where $\underline{c_g}$ is the wave group velocity, $c = |\underline{c_g}|$; $\underline{k}$ the wavenumber vector, $k = |\underline{k}|$; D denotes the total water depth, R the radius of the earth; $\underline{u}$ represents the current velocity (u,v), $\dot{\theta}_{gc}$ the great circle refraction term.

The source term $S = S_{in} + S_{nl} + S_{ds} + S_{bf}$, represents the wind input, the nonlinear wave-wave interaction, the dissipation due to white-capping and bottom friction, respectively (WAMDI, 1988). An implicit integration scheme (WAMDI,1988) is used for the integration of the source functions and a first order upwind differencing and volume control scheme is used for the advective terms. The numerical dispersion inherent in the upwind differencing scheme is considered to give an adequate wave dispersion in storm wave simulation (Hubbert and Wolf,1991). The total water depth and mean current velocity and their gradients are calculated using a barotropic tide and surge model developed at the Proudman Oceanographic Laboratory (Proctor and Flather, 1983), which is based on the momentum and mass conservation equations in depth-averaged form,

$$\frac{\partial\underline{u}}{\partial t} + \underline{u}\cdot\nabla\underline{u} + 2\underline{\Omega}\times\underline{u} + g\nabla\left(\zeta + \frac{p_a}{\rho g}\right) + \frac{\underline{\tau_S} - \underline{\tau_B}}{\rho D} + A_H\nabla^2\underline{u} = 0 , \qquad (5)$$

$$\frac{\partial\zeta}{\partial t} + \nabla\cdot(D\underline{u}) = 0 , \qquad (6)$$

where $\underline{u}$ is the depth averaged current velocity vector, ζ the elevation of the sea surface above its undisturbed level; D represents the total water depth, $\underline{\Omega}$ the planetary angular velocity; $\underline{\tau_S}$ and $\underline{\tau_B}$ are the surface wind stress and bottom stress respectively; ρ is the density of water, p_a the atmospheric pressure; g denotes the gravitational acceleration and A_H is a horizontal eddy viscosity coefficient. The equations are solved by a finite difference scheme on a

staggered grid, with tidal inputs and a gravity wave radiation condition employed at the open boundaries.

At the wave model open boundaries an energy forcing scheme is implemented in an attempt to simulate the propagation of the North Atlantic swells into the model. The scheme uses the significant wave heights at the open boundary grid points, extracted from the wave charts produced by the Met. Office global wave model (75km resolution). Assuming a Pierson-Moskowitz (1964) spectrum for a fully developed sea state and a $\cos^2$ directional spreading function, the 2-D directional wave energy spectra at the open boundaries are specified by

$$\begin{aligned} E(f,\theta) &= 4.99\times10^{-4}\, f^{-5} \exp[-2.00\times10^{-3} H_s^{-2} f^{-4}]\, \frac{2}{\pi}\cos^2(\theta-\theta_w), \qquad \cos(\theta-\theta_w)\geq 0 \\ &= 0, \qquad\qquad \cos(\theta-\theta_w)<0 \end{aligned} \tag{7}$$

where f is the wave frequency, θ the wave direction, H_s the significant wave height and θ_w the wind direction. Use of more elaborate open boundary conditions is possible, but would require more complete data from the large scale wave model.

The model is set up on a latitude and longitude grid covering the European continental shelf region with some parts extended beyond the shelf edge to form a full rectangular area from 45°40'N to 62°20'N and from 15°W to 13°E. The computational grid, shown in Fig.1, has a spacing of 1/3° in latitude and 1/2° in longitude, resulting in a spatial resolution of approximately 35km. The wave action spectra $N(\omega_o,\theta;\underline{x},t)$ are discretized in 26 frequency bins from 0.0418 Hz and with 10% increment. A directional resolution of 15° is adopted in order to study the effects of depth and current refraction. The model is run with a time step of 10 minutes for both propagation and source term integration, which satisfies the CFL stability criterion.

A hindcast study was carried out for the "Great Storm" of October 1987, which tracked NNE across the English Channel and the North Sea causing much damage and disruption in southern England and other parts of Europe. The hourly wind fields used to drive the models were produced from data assimilation runs of the Met. Office limited area

atmospheric model. For the crucial period from 12z 15th to 00z 17th October when the storm passed from Brittany to the central North Sea, an atmospheric model forecast initialized with all data available 'after the event' was used. Wind speeds were converted from 19.5m height to 10m height assuming a logarithmic profile. A two dimensional linear interpolation is used to map the winds to the wave model grid. Initialised with the JONSWAP spectrum (Hasselmann et al.1973), the wave model was run for a 4 day simulation from 00z 14th to 00z 18th October 1987. The surface stress is calculated using the Smith & Banke drag coefficient formula (Smith and Banke 1975), consistent with that used in the tide and surge calculation.

To assess the effects of the open boundary condition and the depth and current refraction scheme, a total of four model runs were performed, with different specifications of open boundary conditions and water depth and currents. Firstly, the model was run without open boundary forcing, using prescribed bathymetry in the region and assuming zero currents. In the second run the open boundary forcing scheme was used but there was still no input of time-varying water depth and current from the surge model, so that the effects of the boundary condition could be examined. To study the effects of wave refraction due to tide and surge motion two more runs were carried out with open boundary wave input, one with both depth and current refraction using hourly water depth and currents from the surge model, and the other with depth refraction only, i.e. using the hourly input of water depth but assuming zero currents. This allowed the relative importance of the depth and the current refraction to be assessed.

3. GEOSAT ALTIMETER DATA AND BUOY MEASUREMENTS

The GEOSAT altimeter, built by the John Hopkins University Applied Physics Laboratory, operated from March 1985 to January 1990. The measurements taken included significant wave height (SWH) and wind speed on the ocean surface (Cheney et al., 1991). The SWH is determined from the slope of the altimeter-returned pulse (Rufenach and Alpers, 1978). The target accuracy of the SWH measured by GEOSAT was specified as 10 percent of the SWH or 0.5m rms, whichever is greater. The wind speed is derived from the backscattered altimeter radar cross section σ_o (dB) by applying an empirically determined algorithm. The accuracy of the wind speed measurement was specified as 1.8 m/s rms over the range from 1 to 18 m/s (MacArthur et al. 1987). Various validation studies and applications of the GEOSAT data showed that these goals were usually met (see, for example, Dobson et al., 1987 and 1990; Shuhy et al., 1987).

The GEOSAT wave height data were first used to identify possible storms in the Northeast Atlantic region during the period from November 1986 to September 1989, which was the majority of the 17 day Exact Repeat Mission (Cheney et al., 1991). In the process, the third week of October 1987 was clearly found to be an interesting storm period for our study. In order to obtain a good GEOSAT data set for comparison with that from the model, the wave height and wind speed data along the sub-satellite tracks in the region of interest were further analyzed using various tests. The "Challenor test" (Challenor et al., 1990) was applied to remove inaccurate data caused by, for example, contamination by returns from land within the altimeter footprint. The SWH values were subsequently corrected using the scheme proposed by Hayne and Hancock (1990), which considers the effects of satellite mis-pointing on radar altimeter measurements, and provides an additive correction to the NOAA-distributed GEOSAT estimates of SWH. The correction to the original SWH values is typically 7 %. However, Carter et al. (1992) found that the original GEOSAT SWH to be underestimated by 13% throughout the range of measurements. Consequently, we assign a conservative error of order 5% on SWH values in our study.

GEOSAT wind speeds were derived using the algorithm proposed by Carter et al.(1992). This method, which is supported by the recent work of Witter and Chelton (1991),

gives more accurate estimates of the wind speed at 10m from the GEOSAT altimeter radar cross-section σ_o (dB) than previously achieved. The rms deviation in wind speeds is 1.46m/s, lower than the 1.7m/s for the smoothed-Brown algorithm reported by Dobson et al.(1987). GEOSAT data along each track are averaged every 5 seconds, which yields a spatial resolution comparable to that of the present model. A complete map of the nine satellite tracks over the European continental shelf region during the time between 00z 14th and 00z 18th October 1987 is shown in Fig.1.

The GEOSAT altimeter provides information over a large area, but, as the satellite was operated in a 17-day repeat (i.e. it flies over the same sea point every 17 days), it does not give time series of sea state parameters for a single storm at fixed locations. For intercomparison of temporal variations of observed wave data with modelled data during the storm of October 1987, we obtained buoy measurements from three Dutch Rijkswaterstaat (RWS) stations in the North Sea and Amoco's Leman platform. The three RWS stations are named K13A, EU0 and AUK. Table 1 and Figure 1 provide locations and water depths at those stations. Significant wave heights and mean wave periods during the "Great Storm" are available for comparison with the data from the wave model. The SWH is calculated from the energy spectrum as $4M_0^{1/2}$ and the mean wave period as M_0/M_1, where M_n is defined by

$$M_n = \int_{f_L}^{f_H} f^n \, E(f) \, df \tag{8}$$

with E(f) representing the sea surface elevation spectrum, and the integration limits f_L=0.00Hz, f_H=0.70Hz.

4. COMPARISON OF MODELLED AND OBSERVED GEOPHYSICAL PARAMETERS

4.1 Model vs GEOSAT: Spatial Variation of Wave Height and Wind Speed

As mentioned earlier, GEOSAT data sets have a wide spatial coverage. This enables us to examine the spatial variation of wave parameters predicted by the wave model and also the winds used to drive the wave model. During the time from 00z 14th to 00z 18th October 1987 a total of nine GEOSAT ground tracks containing wave height information were extracted for the area covered by the model. Wind speed data, however, were only found for eight of the nine subtracks, due to the fact that some values were rejected by the criterion adopted during the "Challenor test". The wave heights were plotted along each GEOSAT ground subtrack against model results in the upper panels of Figs. 2(a) to 2(h) and Fig.2(i). As it takes a maximum of five minutes for GEOSAT to complete each passage over the modelled region, we label each subtrack by the time when it entered the region, rounded up to the nearest minutes for which data can be extracted from the model. Since the model has a time step of 10 minutes, the approximation in time is up to 5 minutes. Hence, the errors due to the temporal approximation are negligible (Monaldo, 1988).

The wave model outputs data at grid points spaced about 35 km apart, whereas the GEOSAT altimeter provides a wind speed and wave height value every second (6.7 km) along the ground track. Five second averages of wind speeds and wave heights were computed, yielding a spatial separation of the data points comparable with the model. A bilinear interpolation scheme was used to extract data from four surrounding grid points in the model for each computed GEOSAT data point. Results from three model runs were plotted for comparison, with increasing complexity of physical representation, ie. the first run with closed boundaries; the second with the open boundary condition and the third including refraction due to tide and surge motions.

To examine how wave data are related to the input wind fields, the wind speeds produced by the Met. Office atmospheric model were compared with the wind speeds computed from the GEOSAT altimeter radar cross sections. A linear interpolation in time was applied to the hourly Met. Office wind data. The results were plotted in the lower panels

of Figs. 2(a) to 2(h). Scatter plots of the SWH and the wind speed may be seen in Figs.3-6. The statistical analysis is performed using the method described in Section (iii), with results summarized in Table 2.

4.2 Model vs Buoy: Time Series of Wave Height and Wave Period

Three-hourly time series of significant wave height and mean wave period at three RWS stations was extracted from a magnetic tape supplied by the RWS, from 00z 14th to 00z 18th October 1987. In addition, hourly data of SWH and mean wave period were available from the LEMAN platform. All the data were plotted against the corresponding values extracted from the nearest grid points in the wave model as shown in Figs.7(a) to 7(d). A bilinear interpolation in space was also used to derive data from the model. However, it produced results similar to those at nearest grid points.

It was found that the (northern) open boundary forcing has little effect at these North Sea stations (because the winds are predominantly from the south and so are the waves), the wave parameters without the open boundary forcing were therefore omitted in the plots. However, in order to examine the relative importance of the depth and current refractions, a statistical analysis was also carried out on the data from the model run with depth refraction only (see Table 3).

4.3 Statistical Analysis

Statistical analyses were performed for each of the parameters of the significant wave height, the mean wave period and the wind speed, using separate buoy and satellite measurements as reference values, respectively. The root mean square error (RMSE), the mean error (ME) and the mean absolute error (MAE) are computed according to the following definitions

$$\text{RMSE} = (\Sigma(X_i - Y_i)^2/N)^{1/2},$$

$$\text{ME} = \Sigma(X_i - Y_i)/N,$$

$$\text{MAE} = \Sigma|X_i - Y_i|/N.$$

The standard deviation (SD), the scatter index (SI) and the linear correlation coefficient (R) are computed using the relations

$$\text{SD} = (\text{RMSE}^2 - \text{ME}^2)^{1/2},$$

$$SI = RMSE \times 100 / \overline{Y},$$

$$R = [\Sigma(X_i-\overline{X})(Y_i-\overline{Y})]/[\Sigma(X_i-\overline{X})^2(Y_i-\overline{Y})^2]^{1/2}.$$

In the above relations and definitions, X_i and Y_i (i=1,2,...,N) denote modelled and observed values respectively, with $\overline{X}$ and $\overline{Y}$ their corresponding averaged values. N is number of comparison points.

5. RESULTS AND DISCUSSIONS

Figs.2(a) to 2(i) show a generally good agreement of the spatial distribution of the modelled and altimeter-derived significant wave heights along each GEOSAT track, particularly when one considers the comparison of corresponding wind fields at the same time. The introduction of the open boundary scheme has to a great extent improved wave height estimates, particularly in areas adjacent to the wave model's open boundaries. This demonstrates that the simple open boundary scheme is effective in accounting for the wave energy input. The influence of the open boundary condition is evident in areas as deep as some 8 degrees in latitude or longitude into the modelled domain (see Tracks 8,9 and portions of Tracks 3,4 and 5 in Figs.2(c)-2(e), 2(h) and 2(i)). However, there are some areas where the results from the wave model prediction and the GEOSAT measurement do not agree. The worst areas are the Skagerrak and Kattegat (Track 2) and along the Norwegian coast (parts of Tracks 4 and 6), where significant differences occurred between the modelled and the GEOSAT altimeter-derived SWH. This appeared to be associated with the errors in wind field specification (see Figs.2(b), 2(d)).

Table 2 shows a comparison of statistical data of SWH hindcast by different model runs, with respect to GEOSAT data, together with the statistical results of wind speeds along GEOSAT tracks in the area. With the open boundary forcing the root mean square error of SWH is reduced by nearly 50%, while the mean error is reduced by almost 1m to under 0.07m. The scatter index is decreased from 41.58 to 22.76 and the correlation coefficient is increased from 0.79 to 0.88, resulting in a SWH statistics very close to that of wind speed. Although analysis of the statistical results indicates little bias in the modelled SWH and wind speed data, the scatter plots (Fig.3-6) show a remarkable underestimation of SWH by the wave model at high wind speeds (where SWH at around 8m). Underestimation by the WAM model of SWH at peak wave heights during heavy storms was reported previously by, for example, WAMDI (1988) and Zambresky (1989). The GEOSAT altimeter has not been verified under high sea state conditions. However, underestimation of GEOSAT SWH has been found in a validation study of a global WAM model (Romeiser, 1992). Guillaume and Mognard (1992) also suggested a mean SWH underestimation of 1.5m by the GEOSAT altimeter for waves higher than (or equal to) 5m, as compared to the VAG model. In our

study, we applied correction schemes (see Section 3) so that errors in GEOSAT SWH were reduced by about 50%. However, a detailed look at the scatter plots of wind speeds (Fig.3) and wave heights (Figs.4-6) together with Figs.2(d) and 2(f) reveals that the biggest discrepancies between modelled and altimeter-derived SWH and wind speed occured near the Norwegian coast. It is possible that the underestimation of SWH by the model was associated with errors in wind field (either speed or direction) specification (from the atmospheric model) in this area. However, we found from intercomparison of Figs.3-6 and GEOSAT tracks in Figs.2 that almost all the other major discrepancies between modelled and altimeter-derived SWH and wind speeds also occured when the satellite flied off the land (e.g. the English Channel, the Skagerrak and Kattegat). This could mean that certain degree of contamination by returns from the land still existed in the altimeter data.

Although the overall wave height statistics have hardly been improved when depth and current refraction due to tides and surges is included, the effects are substantial along some parts of the tracks, with the SWH changed by up to 0.4m at some places with local wave height at around 5m (see Fig.2(f)). An improvement in SWH by depth and current refraction is shown in the southern North Sea (part of Track 6), where good agreement of wind speeds is also found. Effects of the depth and current refraction at locations not covered by GEOSAT tracks will be discussed later in the section.

Comparing time series of the SWH and mean wave period at four buoy stations (Fig.7(a)-(d)), the storm peak significant wave height and wave period seem to be modelled well, except at Station C (AUK), where no records were retrieved. The model spin-up is generally good from the agreement of SWH and mean wave period with the buoy measurements before the first peak. However, there is a consistent underprediction of SWH at Station A (EU0), which could be associated with local winds (cf. Fig.2(e)). At Station C (AUK) there is a time lag in the run-up to the peak sea states, which resulted in a small delay in the peak wave height and period, and this persisted in the relaxation of the sea. This feature is not obviously related to the wind errors (cf. Fig.2(g)).

The model reproduced SWH and mean wave period very well at Station B (K13), though there is a slight delay of the second peak. At Station D (Leman), not far from K13,

the delay of the peak sea states and overestimation of the wave parameters in the subsequent decay of the sea states are quite significant. It may be seen in Fig.2(f) that the local winds seem to be modelled well. A possible explanation is the missing local features in the wave model, as the refraction due to tides and surges did bring the SWH closer to that measured by the buoy (Fig.7(d)) and the GEOSAT altimeter (Fig.2(f)). Figs.7(a)-(d) also demonstrate that the depth and current refraction has more effects at storm peaks in shallow waters. The modulations in SWH and in the mean wave period by tides and surges are between 5% and 10%, which agrees with findings in the previous North Sea study (Tolman, 1991).

The wave model was also run with depth refraction only in order to examine the relative importance of depth and current refraction in the model. Results from the model run with depth refraction only (not shown in the figures) were found to be very close to those from the model run with both depth and current refraction, which implies that the refraction in the present model is predominantly caused by time-varying water depth. This argument only applies to the North Sea, as in our study case the refraction effects were largely found along GEOSAT tracks in the North Sea and at the North Sea buoy stations. The statistical comparison of the depth and current refraction models is summarised in Table 2 and 3.

The spatial variations of SWH and the effects of depth and current refraction are illustrated in Figs.8 and 9. Between the time 06z (Fig.8) and 09z (Fig.9) 16th October, when the storm centre travelled across the English Channel, the refraction appeared in different patterns. At 06z 16th, the refraction was predominantly caused by the interaction of waves and currents, and in the English Channel and eastern Irish Sea. The maximum change in SWH was about 0.4m, which accounted for as much as 40% of the local wave height in the Irish Sea (see Fig.8(a)). Fig.8(b) shows the difference in SWH between model runs with and without depth and current refraction, i.e. the total refraction, as a result of the current refraction being slightly compensated by the depth refraction. Three hours later, however, the storm centre moved to the southern North Sea, and the changes in SWH appeared to be mainly due to the changes in water level. The SWH in the southern North Sea was reduced by up to 0.5m (about 8% of local wave height), while in the Channel it was in the range of -0.2m to +0.3m (up to 10% of local SWH). The combined results of depth and current refraction (Fig.9(b)) shows that the current interaction in fact increased the SWH in the

southern North Sea by about 0.1 to 0.2m. Therefore, it may be concluded that up to 0.5m (or 40%, whichever the lower) changes in SWH may result from either depth or current refraction alone, and the combined effects may amount to a much bigger modulation in SWH in other storm cases than what has been demonstrated in this study.

It should be remembered here that the refraction effects which we are currently examining are caused by the temporal and spatial variation of water depth and currents induced purely by the tide and surge motion, and the so called "no refraction" model in this report actually includes wave refraction due to time-invariant bottom topography. Note that the tide and surge model used in our study calculates depth-averaged currents. The influence of vertical structure of currents on wave model performance remains to be investigated by coupling the wave model with a 3D current model.

6. CONCLUSIONS AND OUTLOOK

A third generation wave model derived from the WAM model with depth and current refraction and an open boundary forcing scheme has been presented in this report. Coupled with a barotropic tide and surge model, the model was used for wave hindcast during the "Great Storm" of October 1987 across the European continental shelf seas. Significant wave heights and wind speeds during the storm period were derived from the GEOSAT altimeter, using some newly developed schemes which further increased the reliability and accuracy of the altimeter data. Spatial distributions of SWH hindcast by the model were compared with the GEOSAT data. The wind speed data used to drive the model were also compared the wind speeds derived from the GEOSAT altimeter in order to assess the accuracy of the wave hindcast in relation to the quality of the wind fields used. This was complemented by a time series comparison of the modelled wave data with buoy measurements at four North Sea stations.

The wave model performed quite satisfactorily, except in areas near the Norwegian coast and in the Skagerrak and Kattegat, where significant discrepancies in modelled and altimeter-derived SWH occurred. This was found to be strongly associated with errors in local wind field specification. Substantial improvements in the modelled wave parameters resulted from the introduction of the open boundary energy forcing scheme, with the influence of the open boundary condition being evident in areas as deep as 8 degrees in latitude or longitude into the modelled region. Due to the open boundary scheme the root mean square error of SWH is reduced by nearly 50% and the mean error by almost 1m to under 0.07m, as compared with GEOSAT data. As a result, the corresponding scatter index and the correlation coefficient have become comparable to those of wind speeds. However, time series of SWH and mean wave height revealed a lag of the hindcast storm peaks at some buoy stations and subsequent overestimation in the decay of the seas. In the scatter plots a remarkable underestimation of SWH by the wave model at peak wave heights has been found for waves at around 8m (near the Norwegian coast). This could also be related to the errors in the wind fields (either wind direction or speed).

The effects of the depth and current refraction due to tides and surges are visible along

some GEOSAT tracks and in the time series plots of wave parameters at three shallower water stations. It is also evident that detailed local variations of SWH were modelled better using the refraction scheme. In the North Sea, the refraction was found to be dominated by that due to time-varying water depth, and the effects are more significant at storm peaks and in shallow water than at other time and in deeper water. The modulations in SWH and the mean wave period by tides and surges are between 5% and 10%, consistent with previous studies. In the Irish Sea (where moderate waves were present) the refraction was predominantly caused by wave-current interaction, resulting in up to 40% change of SWH. In the English Channel, however, depth and current refraction appeared to be equally important (each about 10% of local SWH). In summary, separate depth and current effect may each modulate SWH by up to 0.5m (or 40%, whichever the lower), their combined effects may amount to much bigger changes in SWH than what has been shown here under other storm conditions.

Depth-averaged currents from a barotropic storm surge model were used in our study and had little influence on wave refraction. It would be of interest to couple the wave model to a 3D current model to examine the effects of more realistic vertical current profiles on waves. The wave model with depth and current refraction scheme will next be fully coupled with the tide and surge model, allowing various two-way interaction processes to be taken into account. The resolution both in time and in space will also be increased to treat more intense and fast developing storms. It is expected that the combined wave-tide-surge model will give more accurate forecasts of waves and sea surface elevations and currents.

ACKNOWLEDGEMENTS

This work was partly funded by the U.K. Ministry of Agriculture, Fisheries and Food. The authors would like to thank Dr. P.L. Woodworth and members of the WAM Group for useful discussions and comments on this work. Thanks also go to Mlle. M.-C. Arent, a student at POL from the John Moores University Liverpool, who processed GEOSAT data provided by the U.S. National Oceanic and Atmospheric Administration. Buoy measurements were provided by the Dutch Rijkswaterstaat and the Amoco Company. The U.K. Met. Office supplied wind and wave data.

REFERENCES

Aranuvachapun, S. (1977) Wave Refraction in the Southern North Sea, Ocean Engineering, vol.4, 91-99.

Bauer, E., Hasselmann, S., Hasselmann, K. and Graber, H.C. (1992) Validation and Assimilation of Seasat Altimeter Wave Heights Using the WAM Wave Model, Journal of Geophysical Research, Vol.97, No.C8, 12671-12683.

Bretherton, F.P. and Garrett, C.J.R. (1969) Wavetrains in Homogeneous Moving Media, Proceedings of the Royal Society of London, A, Vol.302, 529-554.

Carter, D.J.T., Challenor, P.G. and Srokosz, M.A. (1992) An Assessment of GEOSAT Wave Height and Wind Speed Measurements, Journal of Geophysical Research, Vol.97, No.C7, 11383-11392.

Challenor, P.G., Foale, S. and Webb, D.J. (1990) Seasonal Changes in the Global Wave Climate Measured by the GEOSAT Altimeter, International Journal of Remote Sensing, 11(12), 2205-2213.

Cheney, R.E., Doyle, N.S., Douglas, B.C., Agreen, R.W., Miller, L., Timmerman, E.L. and McAdoo, D.C. (1991) The Complete Geosat Altimeter GDR Handbook, The U.S. National Oceanic and Atmospheric Administration Manual NOS NGS 7.

Clayson, C.H. and Ewing, J.A. (1988) Directional Wave Data Recorded in the Southern North Sea, Institute of Oceanographic Sciences Deacon Laboratory, Report No.258, 70pp.

Dobson, E., Monaldo, F., Goldhirsh, J. and Wilkerson, J. (1987) Validation of GEOSAT Altimeter-Derived Wind Speeds and Significant Wave Heights Using Buoy Data, Johns Hopkins APL Technical Digest, 8, 222-233.

Dobson, E.B. and Chaykovsky, S.P. (1990) GEOSAT Wind and Wave Measurements During LEWEX, Johns Hopkins APL Technical Digest, Vol.11, No.3-4, 408-413.

Guillaume, A. and Mognard, N.M. (1992) A New Method for the Validation of Altimeter-Derived Sea State Parameters with Results from Wind and Wave Models, Journal of Geophysical Research, Vol.97, No.C6, 9705-9717.

Hasselmann, K., Barnett, T.B., Bouws, E., Carson, H., Cartwright, D.E., Enke, K., Ewing, J.A., Gienapp, H., Hasselmann, D.E., Kruseman, P., Meerburg, A., Müller, P., Olbers, D.J., Richter, K., Sell, W. and Walden, H. (1973) Measurements of Wind-Wave Growth and Swell Decay During the Joint North Sea Wave Project (JONSWAP), Deutschen Hydrographischen Zeitschrift Reihe A(8) No.12, 95pp.

Hasselmann, K., Hasselmann, S., Bauer, E., Brüning, C., Lehner, S., Graber, H. and Lionello, P. (1988) Development of a Satellite SAR Image Spectra and Altimeter Wave Height Data Assimilation System for ERS-1, European Space Agency Contract Report ESRIN 6875/87 HGE-I(SC), Max-Planck-Institut für Meteorologie, Hamburg.

Hayne, G.S. and Hancock, D.W. (1990) Corrections for the Effects of Significant Wave Height and Attitude on GEOSAT Radar Altimeter Measurements, Journal of Geophysical Research-Oceans, 95(C3), 2837-2842.

Hubbert, K.P. and Wolf, J. (1991) Numerical Investigation of Depth and Current Refraction of Waves, Journal of Geophysical Research-Oceans, 96(C2), 2737-2748.

Janssen, P.A.E.M., Lionello, P., Reistad, M. and Hollingsworth, A. (1987) A Study of the Feasibility of Using Sea and Wind Information from ERS-1 Satellite, Part 2: Use of Scatterometer and Altimeter Data in wave Modelling and Assimilation, European Space Agency Contract Report ESRIN 6297/86/HGE-I(SC), ECMWF, Reading, U.K.

MacArthur, J.L., Marth Jr., P.C. and Wall, J.G. (1987) The GEOSAT Radar Altimeter, Johns Hopkins University APL Technical Digest, No.2, Vol.8, 176-181.

Meteorological Office Report (1988) The Storm of 15/16 October 1987, United Kingdom, 17pp.

Monaldo, F. (1988) Expected Differences Between Buoy and Radar Altimeter Estimates of Wind Speed and Significant Wave Height and Their Implications on Buoy-Altimeter Comparisons, Journal of Geophysical Research-Oceans, 93(C3), 2285-2302.

Pierson, W.J.,Jr. and Moskowitz, L. (1964) A proposed Spectral Form for Fully Developed Wind Seas Based on the Similarity Theory of S.A.Kitaigorodskii, Journal of Geophysical Research, 69, 5181-5190.

Proctor, R. and Flather, R.A. (1983) Routine Storm Surge Forecasting Using Numerical Models: procedures and computer programs for use on the CDC CYBER 205 at the British Meteorological Office, Institute of Oceanographic Sciences Report No.167, 171pp.

Romeiser, R. (1992) Validation of the WAM Wave Prediction Model by GEOSAT Wave Height Data, submitted to Journal of Geophysical Research.

Rufenach, C.L. and Alpers, W.R. (1978) Measurement of Ocean Wave Heights Using the Geos 3 Altimeter, Journal of Geophysical Research, 83, 5011-5018.

Shuhy, J.L., Grunes, M.R., Uliana, E.A. and Choy, L.W. (1987) Comparison of GEOSAT and Ground Truth Wind and Wave Observations: Preliminary Results, Johns Hopkins APL Technical Digest, 8(2), 219-221.

Smith, S.D. and Banke, E.G. (1975) Variation of the Sea Surface Drag Coefficient with Wind Speed, Quarterly Journal of Royal Meteorological Society 101, 665-673.

Sverdrup, H.U. and Munk, M.H. (1947) Wind Sea and Swell: Theory of Relations for Forecasting, Hydrographic Office Publication 601, U.S. Navy Hydrographic Office, Washington, D.C., 44pp.

The SWAMP Group (1985) Sea Wave Modelling Project (SWAMP), Part 1: Principal Results and Conclusions, Ocean Wave Modelling, Plenum Press, 256pp.

Tolman, H.L. (1991) Effects of Tides and Storm Surges on North Sea Wind Waves, Journal of Physical Oceanography, Vol. 21, No.6, 766-781.

Vincent, C.E. (1979) The Interaction of Wind-Induced Sea Waves with Tidal Currents, Journal of Physical Oceanography, vol.9, 748-755.

The WAMDI Group (1988) The WAM Model-A Third Generation Ocean Wave Prediction Model, Journal of Physical Oceanography, Vol.18, No.12, 1775-1810.

Witter, L.D. and Chelton, B.D. (1991) A Geosat Altimeter Wind Speed Algorithm and a Method for Altimeter Wind Speed Algorithm Development, Journal of Geophysical Research-Oceans, 96(C5), 8853-8860.

Wolf, J., Hubbert, K.P. and Flather, R.A. (1988) A Feasibility Study for the Development of a Joint Surge and Wave Model, Proudman Oceanographic Laboratory Report No.1, 109pp.

Zambresky, L. (1989) A Verification Study of the Global WAM model, December 1987-November 1988, ECMWF Technical Report No.63, 86pp, Reading, U.K..

CAPTIONS TO THE FIGURES

Fig.1 European Continental Shelf (CSXP) wave model grid, GEOSAT tracks and locations of buoys.(A-EU0, B-K13, C-AUK and D-LEMAN.)

Figs.2(a)-(i)

Comparison of modelled SWHs (upper panel in each figure) and wind speeds (lower panel in each figure) with those derived from GEOSAT altimeter, along Tracks 1-8. (• • • • measured data; ------ modelled data without open boundary forcing; —— modelled data with open boundary forcing; *—*—* modelled data with depth and current refraction due to tides and surges.) The cross in 2(f) indicates buoy measurement at Station D. No wind speed comparison for Track 9 in 2(i).

Fig.3 Scatter plot of wind speeds used in the wave model against wind speeds derived from GEOSAT altimeter measurement, with corresponding statistical data.

Fig.4 Scatter plot of SWHs hindcasted by the wave model (without open boundary forcing) against SWHs derived from GEOSAT altimeter measurement, with corresponding statistical data.

Fig.5 Scatter plot of SWHs hindcasted by the wave model (with open boundary forcing) against SWHs derived from GEOSAT altimeter measurement, with corresponding statistical data.

Fig.6 Scatter plot of SWHs hindcasted by the wave model (with depth and current refraction due to tide and surge motion) against SWHs derived from GEOSAT altimeter measurement, with corresponding statistical data.

Figs.7(a)-(d)

Time series of SWH (upper panel in each figure) and mean wave period (lower panel in each figure) at Stations A-D. (• • • • buoy measurement; —— modelled data without depth and current refraction due to tides and surges; *—*—* modelled data

with depth and current refraction due to tides and surges.)

Fig.8(a) Significant Wave Height (contour interval 0.5m) and mean wave direction at 06z 16th October 1987.

Fig.8(b) Difference in significant wave height between model runs with and without depth and current refraction at 06z 16th October 1987.

Fig.9(a) Same as Fig.8(a) but at 09z 16th October 1987.

Fig.9(b) Same as Fig.8(b) but at 09z 16th October 1987.

CAPTIONS TO THE TABLES

Table 1. Stations used for wave model verification.(RWS = Rijkswaterstaat)

Table 2. Statistical comparison of SWH and wind speed for different model runs, using GEOSAT data as references.

Table 3. Statistical comparison of SWH and mean wave period for different model runs, using buoy data as references.

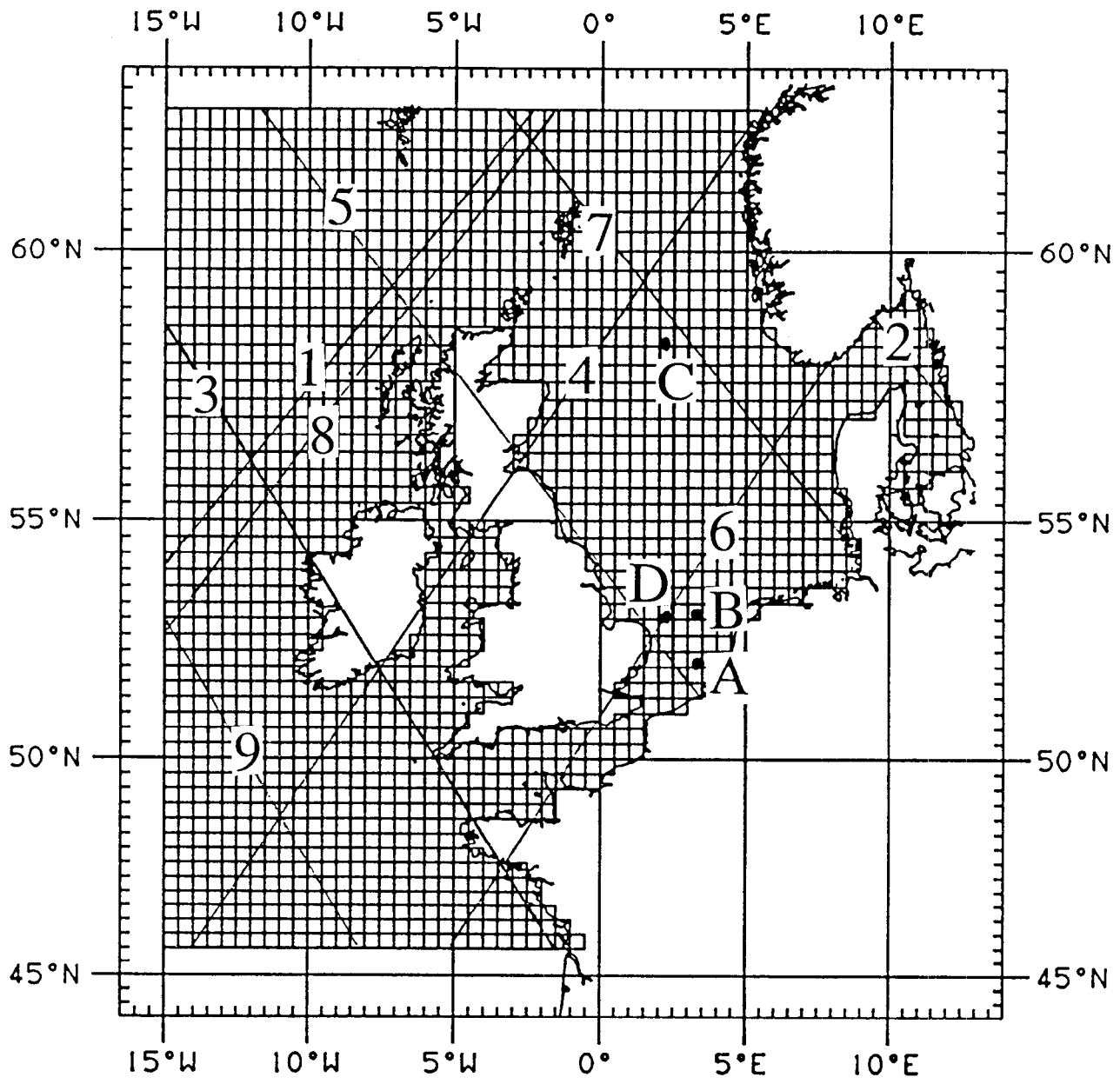

CSXP MODEL

Fig.1

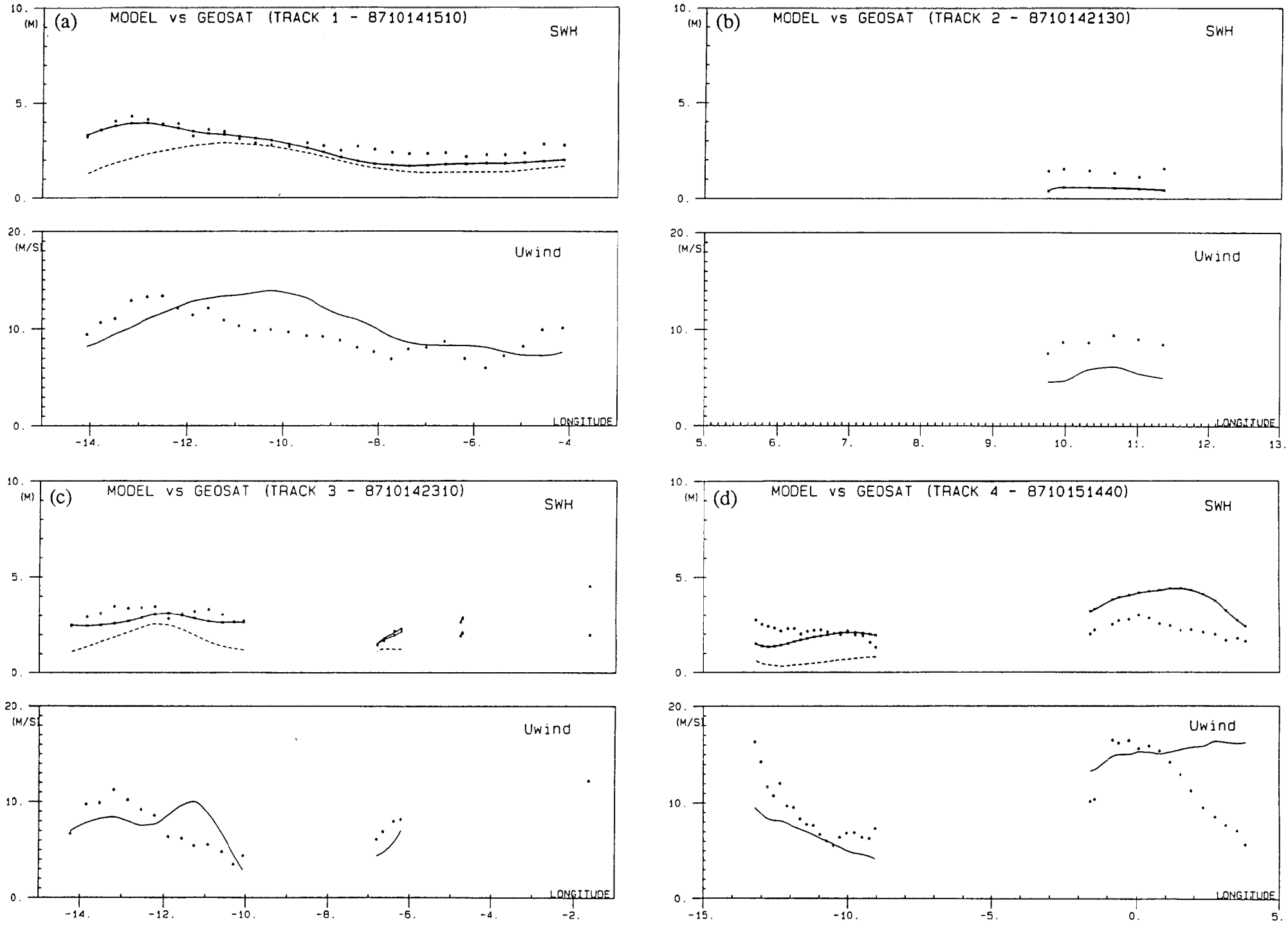
(a) MODEL vs GEOSAT (TRACK 1 - 8710141510)
SWH
(M)
10.
5.
0.
Uwind
(M/S)
20.
10.
0.
LONGITUDE
-14.
-12.
-10.
-8.
-6.
-4.
(b) MODEL vs GEOSAT (TRACK 2 - 8710142130)
SWH
Uwind
5.
6.
7.
8.
9.
10.
11.
12.
13.
(c) MODEL vs GEOSAT (TRACK 3 - 8710142310)
SWH
Uwind
-2.
(d) MODEL vs GEOSAT (TRACK 4 - 8710151440)
SWH
Uwind
-15.
-5.
0.
5.

Figs.2(a)-(d)

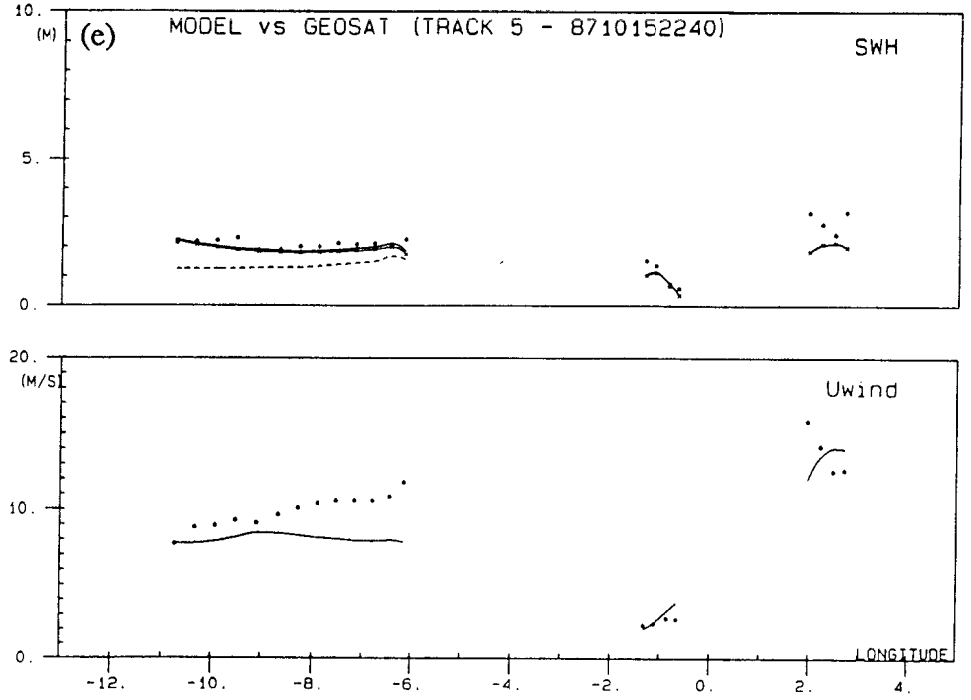
(e)
MODEL vs GEOSAT (TRACK 5 - 8710152240)
SWH
(M)
10.
5.
0.
Uwind
(M/S)
20.
10.
0.
LONGITUDE
-12.
-10.
-8.
-6.
-4.
-2.
0.
2.
4.

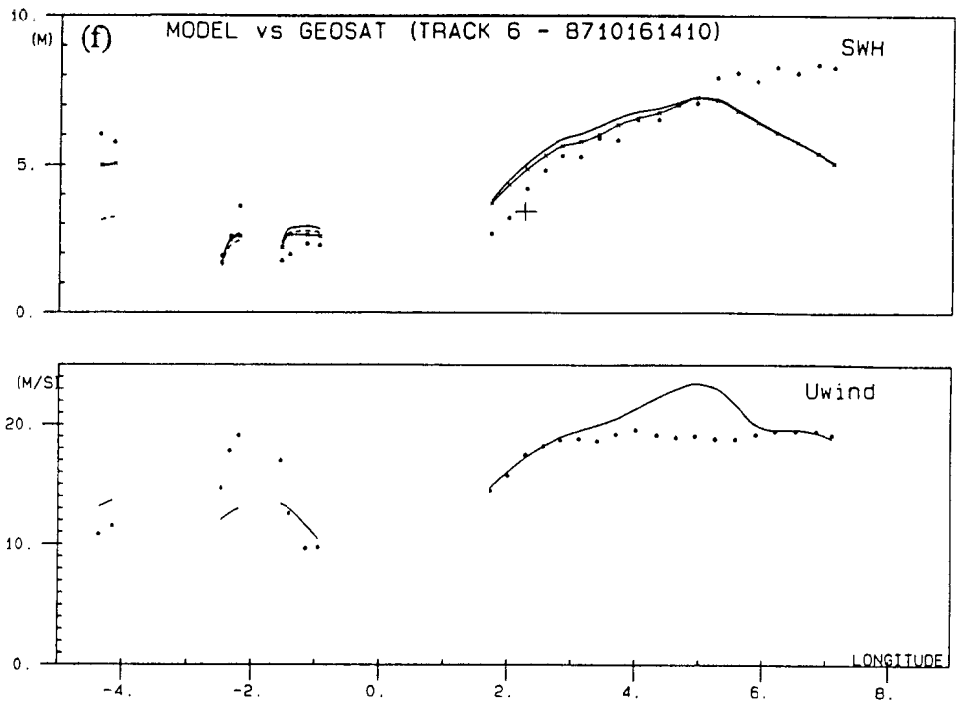
(f)
MODEL vs GEOSAT (TRACK 6 - 8710161410)
SWH
(M)
10.
5.
0.
Uwind
(M/S)
20.
10.
0.
LONGITUDE
-4.
-2.
0.
2.
4.
6.
8.

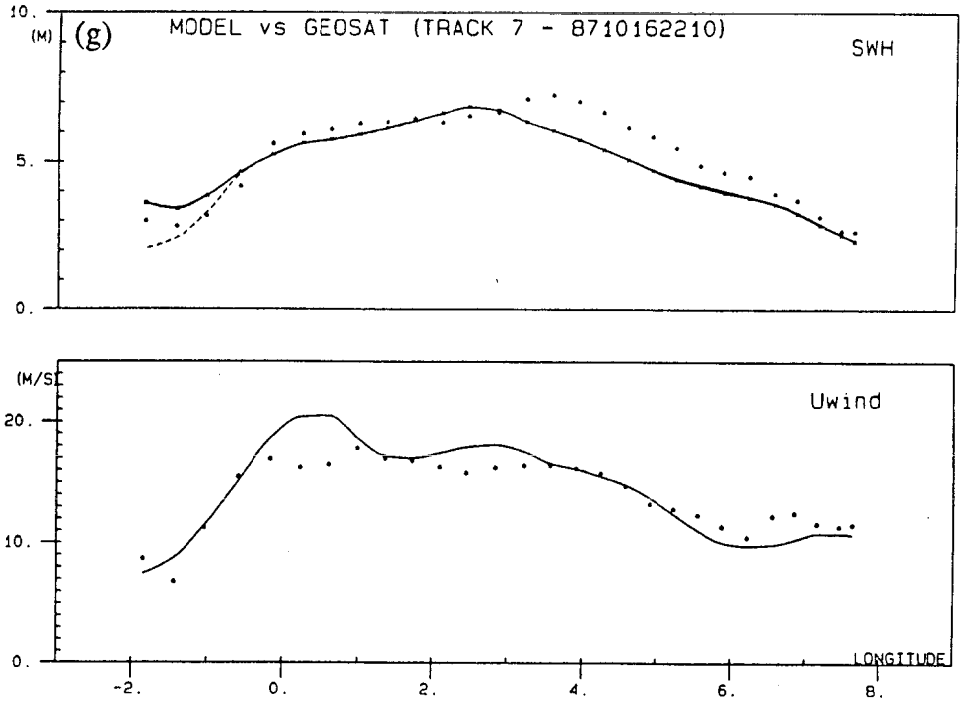
(g)
MODEL vs GEOSAT (TRACK 7 - 8710162210)
SWH
(M)
10.
5.
0.
Uwind
(M/S)
20.
10.
0.
LONGITUDE
-2.
0.
2.
4.
6.
8.

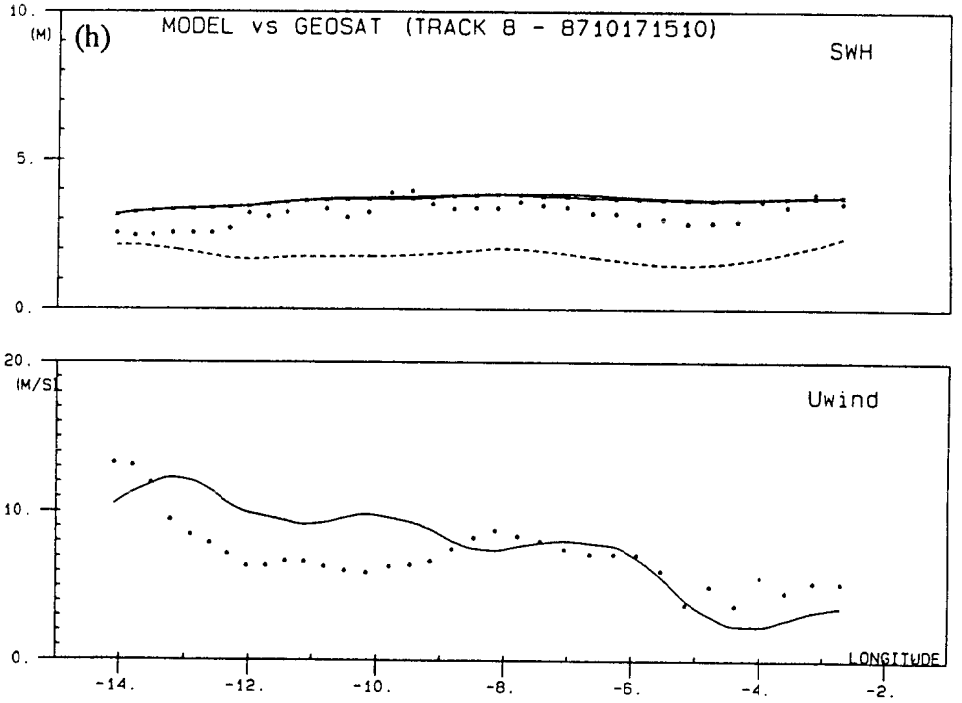
(h)
MODEL vs GEOSAT (TRACK 8 - 8710171510)
SWH
(M)
10.
5.
0.
Uwind
(M/S)
20.
10.
0.
LONGITUDE
-14.
-12.
-10.
-8.
-6.
-4.
-2.

Figs.2(e)-(h)

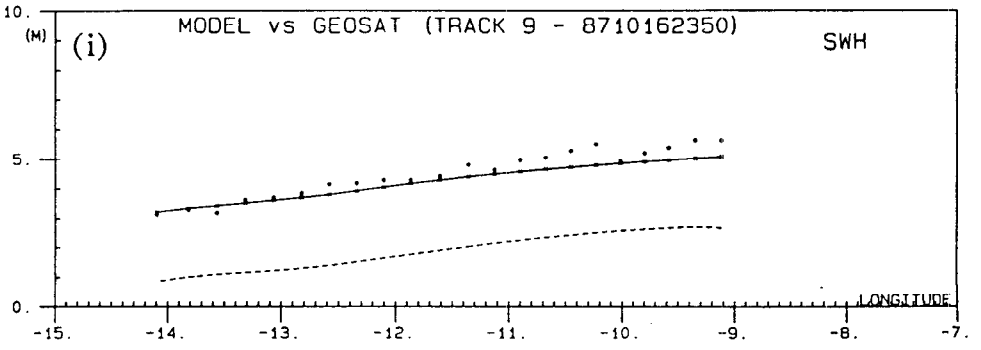
10.
(M)
(i)
MODEL vs GEOSAT (TRACK 9 - 8710162350)
SWH
5.
0.
LONGITUDE
-15.
-14.
-13.
-12.
-11.
-10.
-9.
-8.
-7.

Fig.2(i)

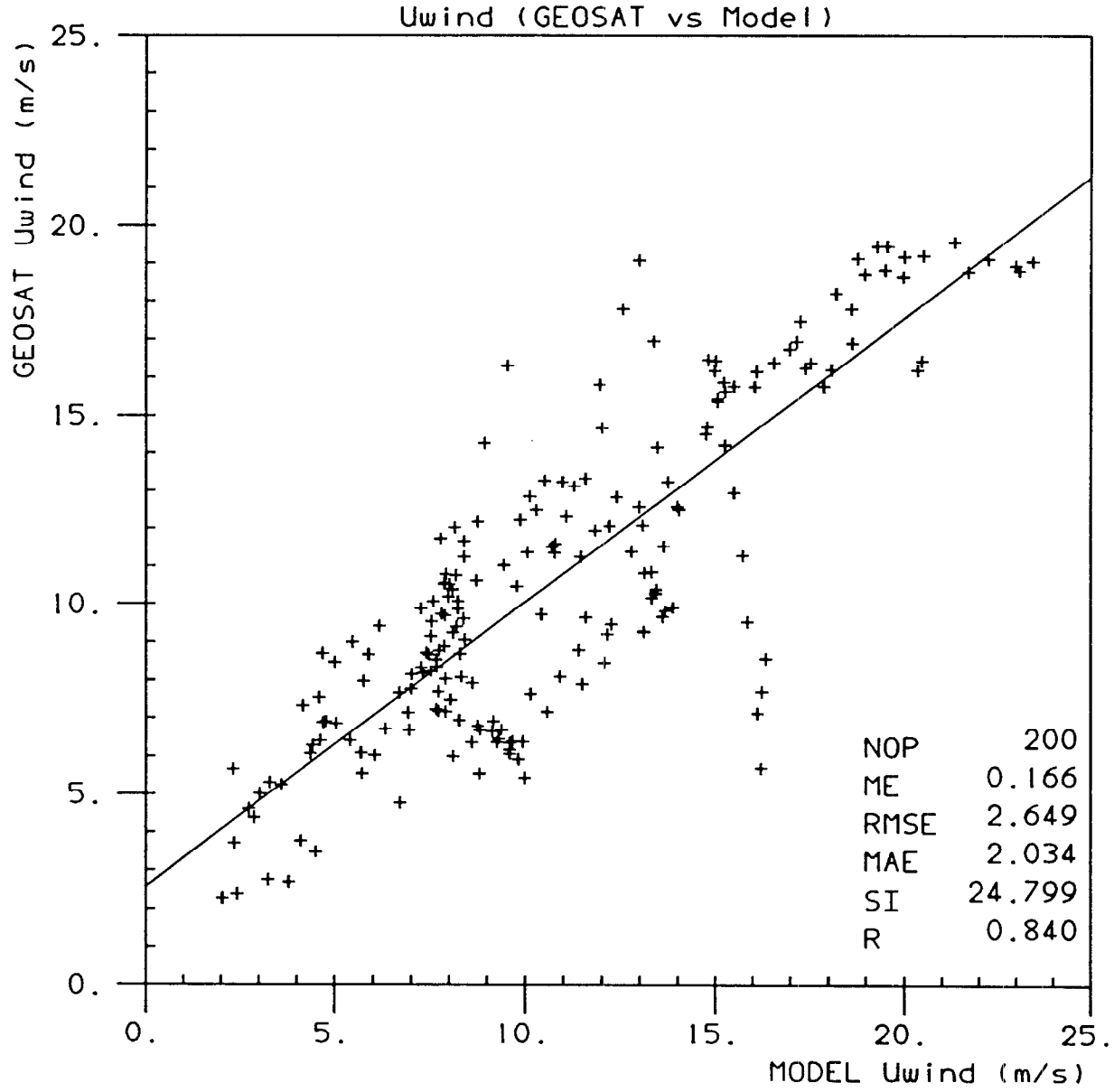
Uwind (GEOSAT vs Model)
GEOSAT Uwind (m/s)
MODEL Uwind (m/s)
0.
5.
10.
15.
20.
25.
NOP 200
ME 0.166
RMSE 2.649
MAE 2.034
SI 24.799
R 0.840

Fig.3

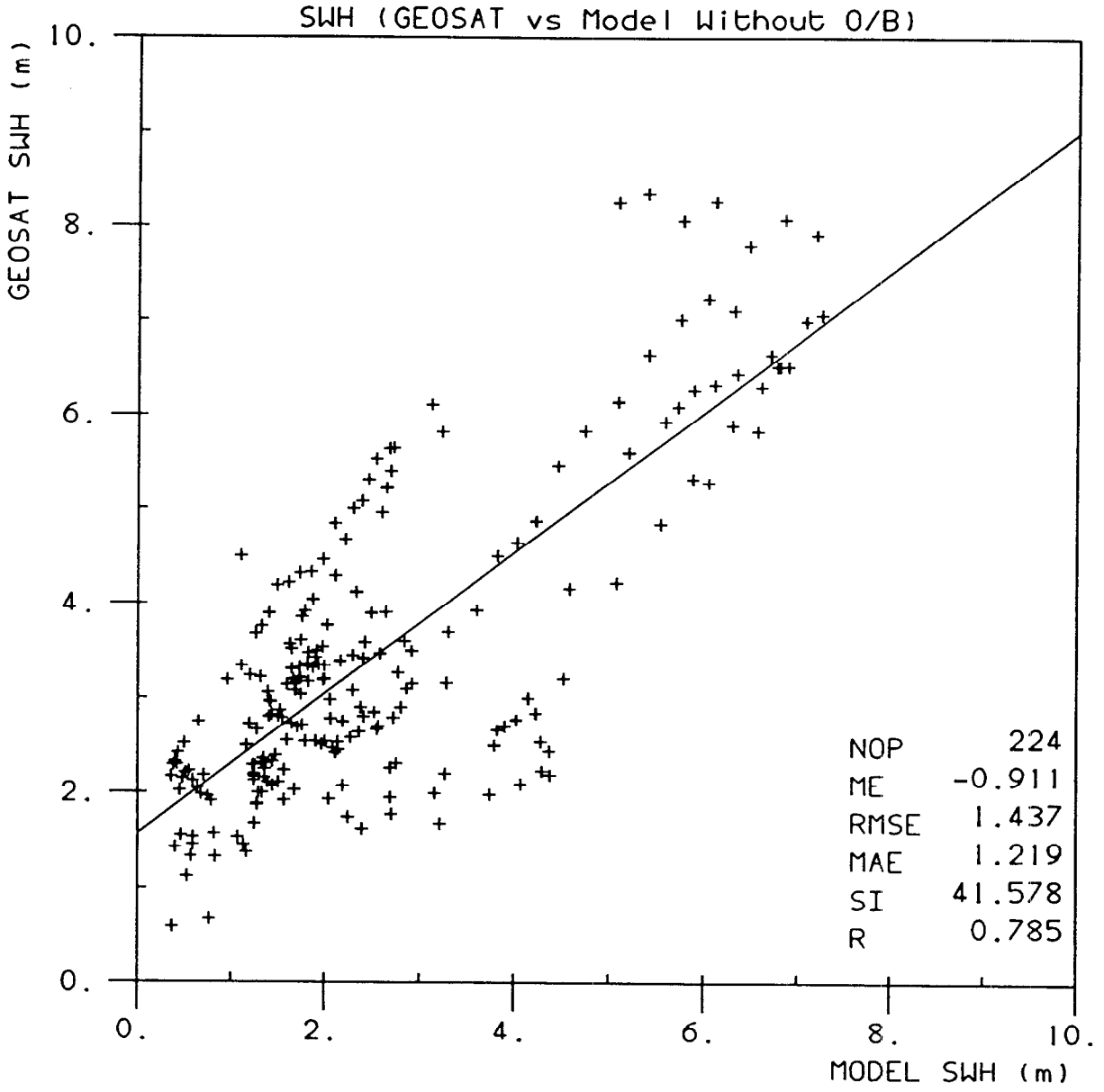
SWH (GEOSAT vs Model Without O/B)
GEOSAT SWH (m)
MODEL SWH (m)
0.
2.
4.
6.
8.
10.
NOP 224
ME -0.911
RMSE 1.437
MAE 1.219
SI 41.578
R 0.785

Fig.4

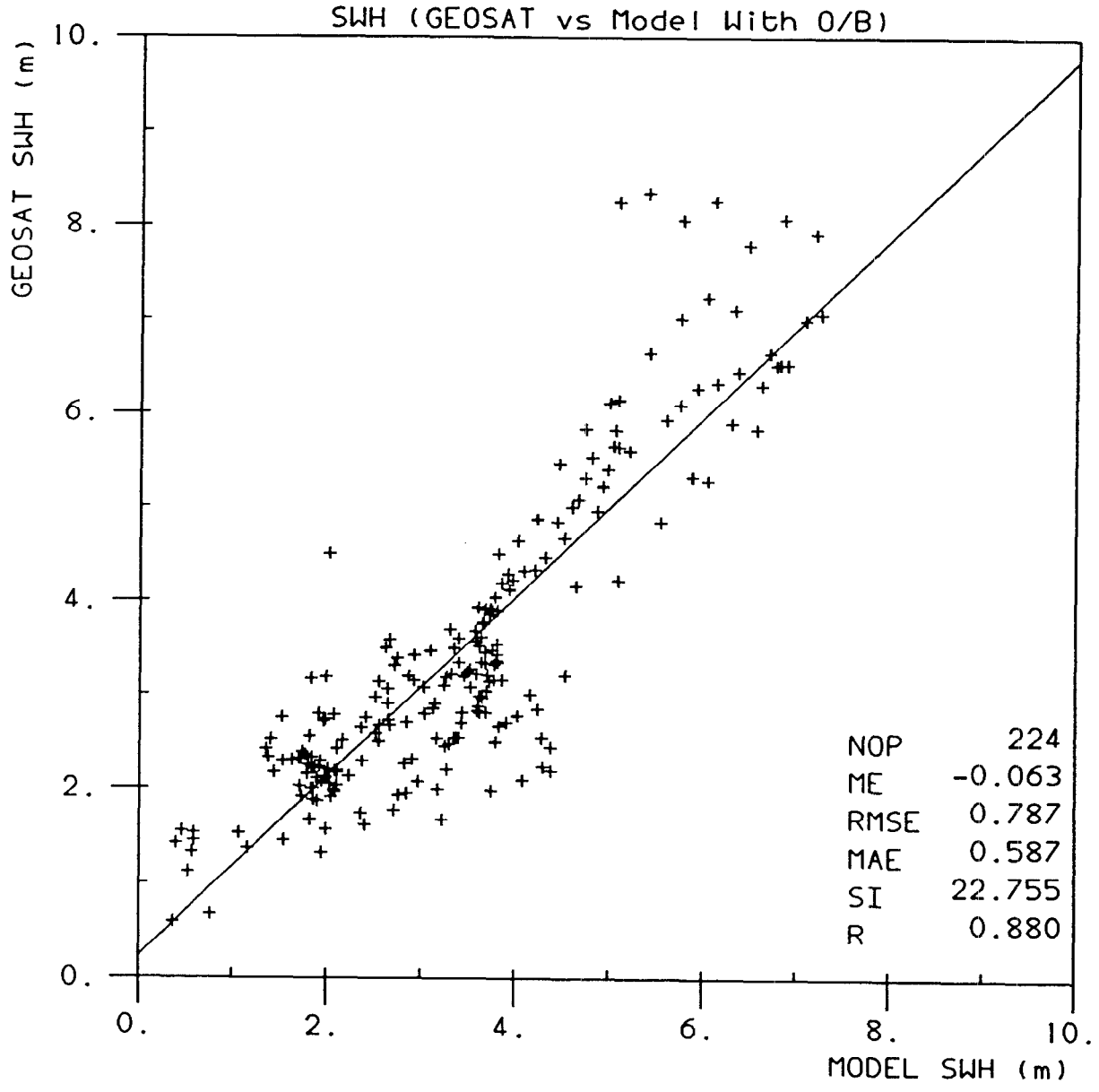
SWH (GEOSAT vs Model With O/B)
GEOSAT SWH (m)
MODEL SWH (m)
0.
2.
4.
6.
8.
10.
NOP 224
ME -0.063
RMSE 0.787
MAE 0.587
SI 22.755
R 0.880

Fig.5

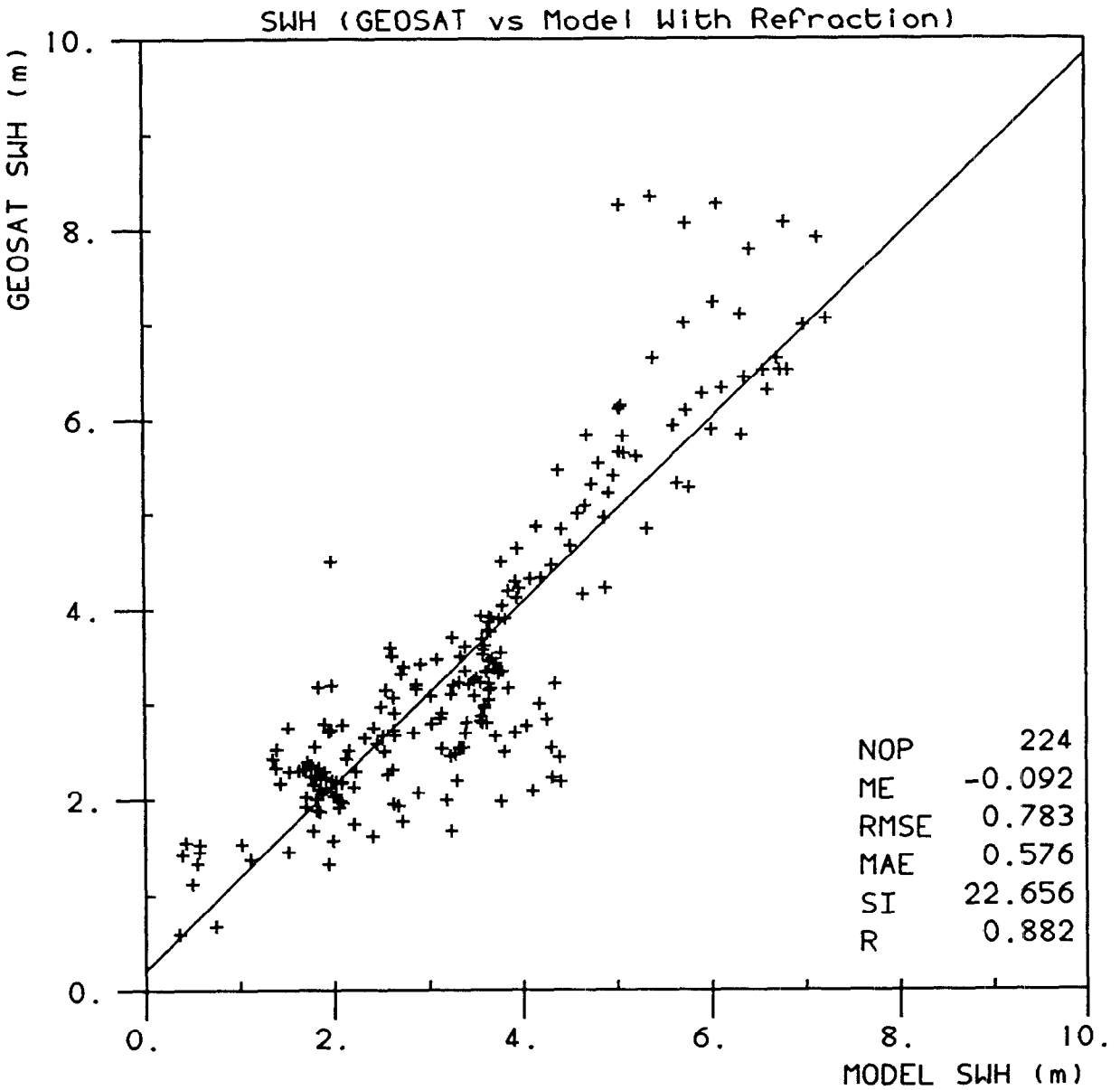
SWH (GEOSAT vs Model With Refraction)
GEOSAT SWH (m)
MODEL SWH (m)
0.
2.
4.
6.
8.
10.
NOP 224
ME -0.092
RMSE 0.783
MAE 0.576
SI 22.656
R 0.882

Fig.6

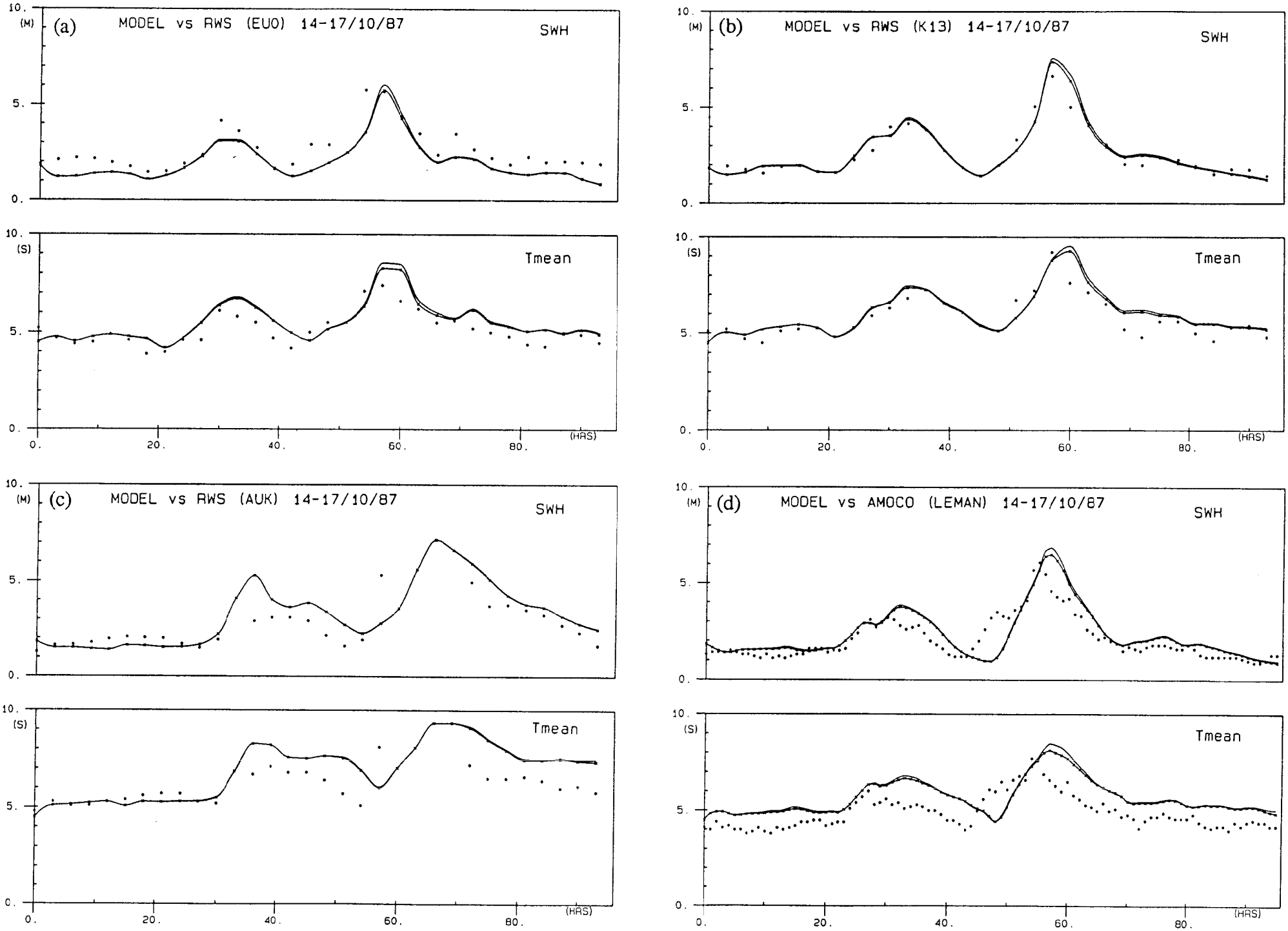
(a) MODEL vs RWS (EUO) 14-17/10/87
SWH
Tmean
(b) MODEL vs RWS (K13) 14-17/10/87
SWH
Tmean
(c) MODEL vs RWS (AUK) 14-17/10/87
SWH
Tmean
(d) MODEL vs AMOCO (LEMAN) 14-17/10/87
SWH
Tmean
(M)
(S)
(HRS)
0.
5.
10.
20.
40.
60.
80.

Figs.7(a)-(d)

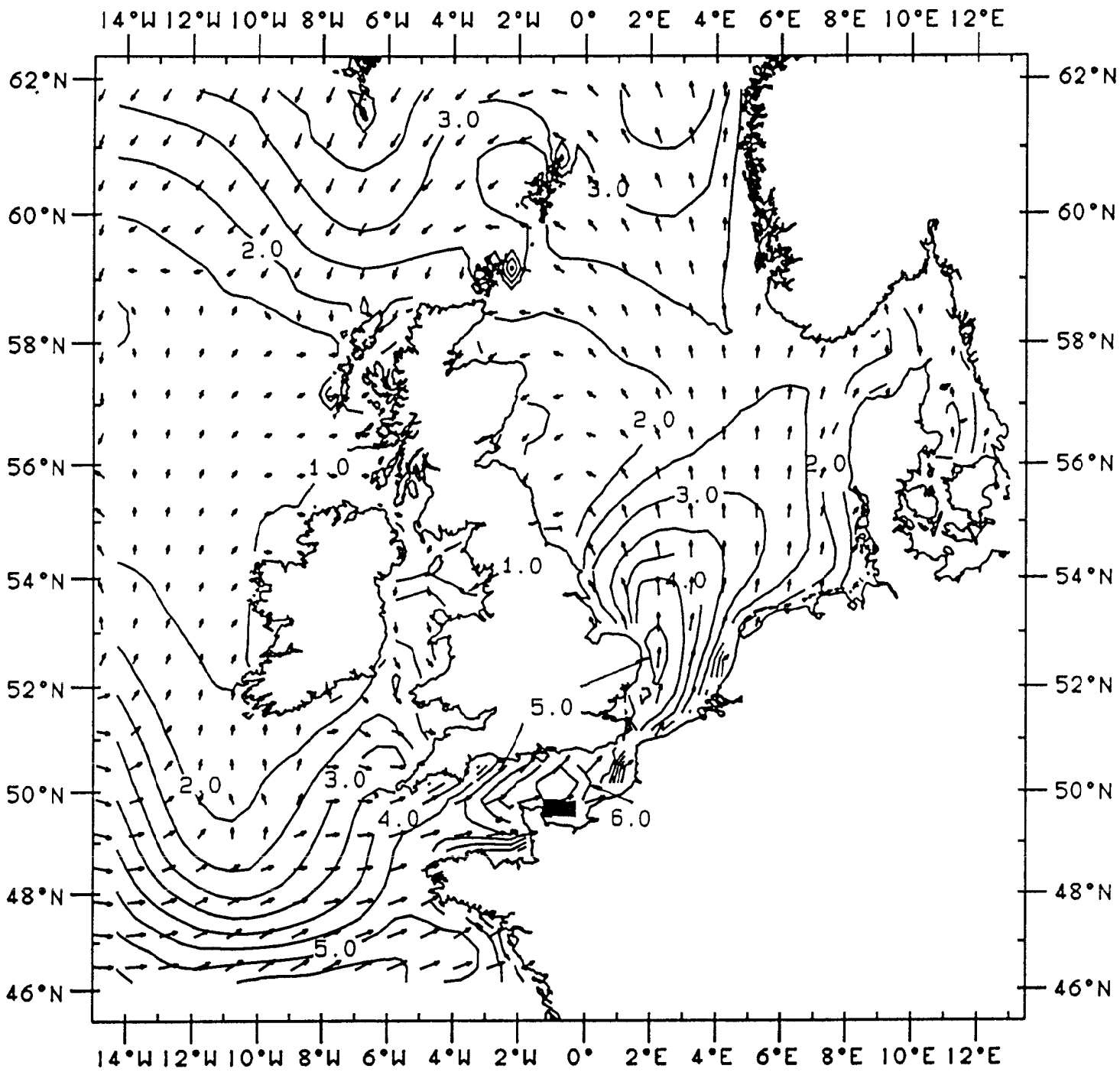
14°W 12°W 10°W 8°W 6°W 4°W 2°W 0° 2°E 4°E 6°E 8°E 10°E 12°E
62°N
60°N
58°N
56°N
54°N
52°N
50°N
48°N
46°N
3.0
3.0
2.0
2.0
1.0
2.0
3.0
1.0
4.0
5.0
2.0
3.0
4.0
6.0
5.0

Fig.8(a)

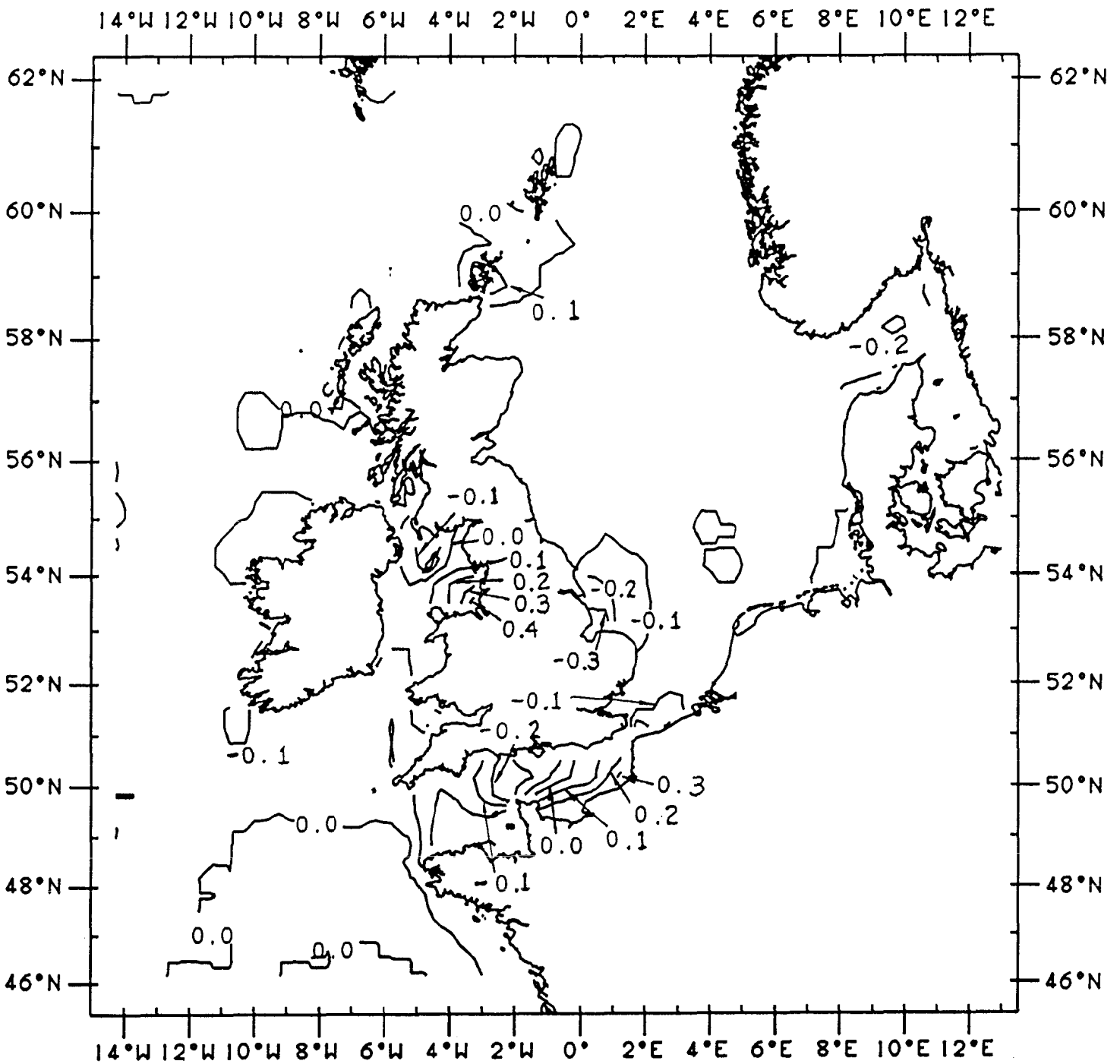
14°W 12°W 10°W 8°W 6°W 4°W 2°W 0° 2°E 4°E 6°E 8°E 10°E 12°E
62°N
60°N
58°N
56°N
54°N
52°N
50°N
48°N
46°N
0.0
0.1
-0.2
-0.1
0.0
0.1
0.2
0.3
0.4
-0.2
-0.1
-0.3
-0.1
-0.2
-0.1
0.3
0.2
0.1
0.0
-0.1
0.0
0.0

Fig.8(b)

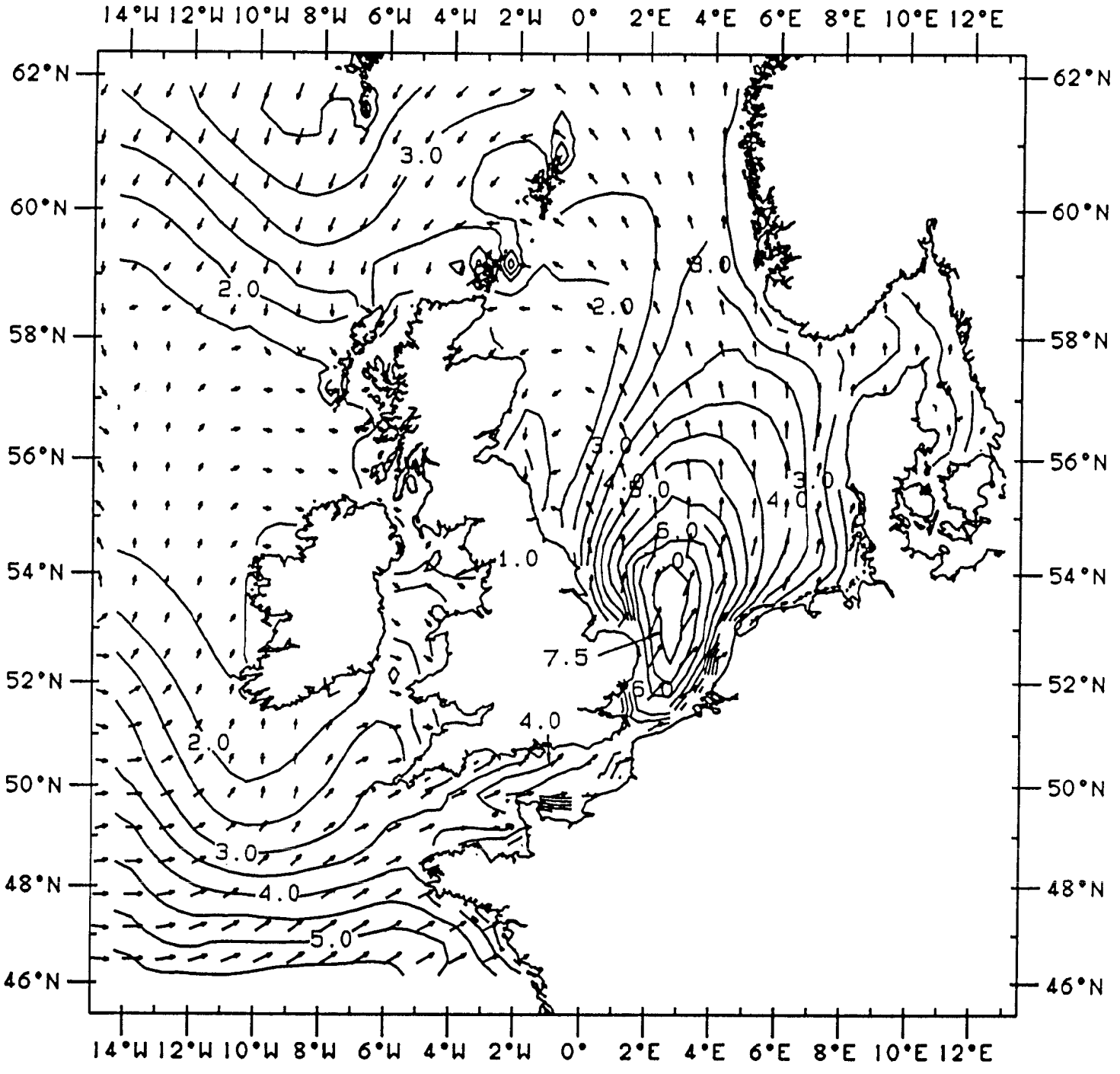
14°W 12°W 10°W 8°W 6°W 4°W 2°W 0° 2°E 4°E 6°E 8°E 10°E 12°E
62°N
60°N
58°N
56°N
54°N
52°N
50°N
48°N
46°N
3.0
2.0
2.0
8.0
3.0
4.0
3.0
8.0
6.0
1.0
7.5
6.0
4.0
2.0
3.0
4.0
5.0

Fig.9(a)

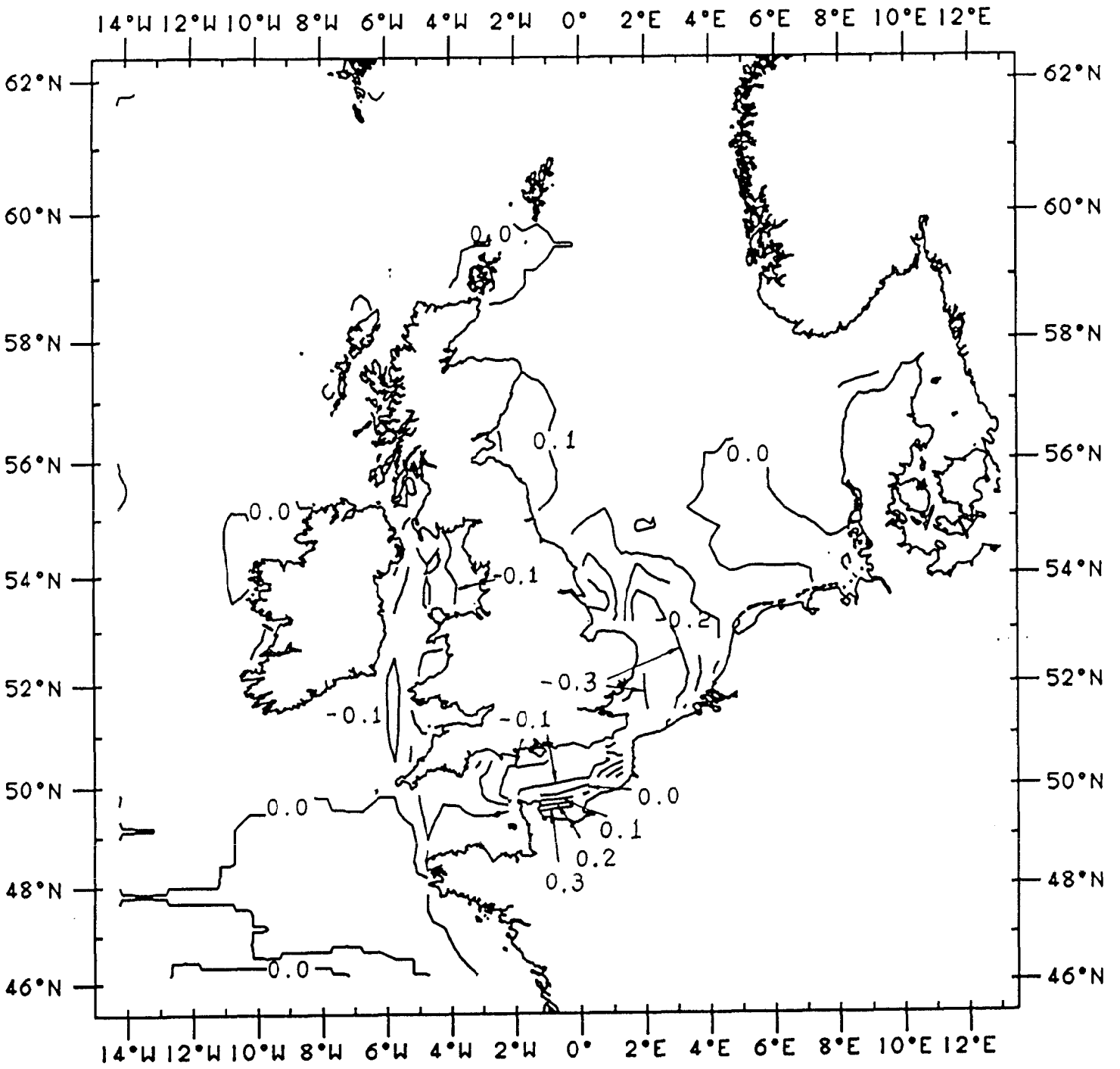
14°W 12°W 10°W 8°W 6°W 4°W 2°W 0° 2°E 4°E 6°E 8°E 10°E 12°E
62°N
60°N
58°N
56°N
54°N
52°N
50°N
48°N
46°N
0.0
0.1
0.0
0.0
-0.1
0.2
-0.3
-0.1
-0.1
0.0
0.0
0.1
0.2
0.3
0.0

Fig.9(b)

Station Name	Latitude (N)	Longitude (E)	Water Depth (M)	Source
A EU0	51°59.55'	3°16.35'	25	RWS
B K13	53°13.10'	3°13.20'	31	RWS
C AUK	58°23.59'	2°3.56'	74	RWS
D LEMAN	53°3.33'	2°14.13'	32	AMOCO

Table 1.

	RMSE (m,m/s)	ME (m,m/s)	MAE (m,m/s)	SD (m,m/s)	Scatter Index	Correlat'n Coeffic't
SWH (Without O/B)	1.437	-0.911	1.219	1.111	41.58	0.785
SWH (With O/B)	0.787	-0.063	0.587	0.784	22.76	0.880
SWH (Refraction)	0.783	-0.092	0.576	0.778	22.66	0.882
SWH (Depth Ref'n)	0.788	-0.085	0.582	0.783	22.80	0.880
Wind Speed	2.649	0.166	2.034	2.644	24.80	0.840
Number of Data Points: 224 (SWH), 200 (Wind Speed). Mean GEOSAT Values: SWH = 3.456 (m), Uwind = 10.68 (m/s).						

Table 2.

		RMSE (m,s)	ME (m,s)	MAE (m,s)	SD (m,s)	Scatter Index	Correlation Coefficient
Model Without Refraction	SWH	0.745	0.112	0.557	0.737	32.15	0.83
	Tm	0.984	0.660	0.839	0.730	18.79	0.77
Model With Refraction	SWH	0.724	0.060	0.533	0.722	30.89	0.83
	Tm	0.924	0.602	0.789	0.701	17.64	0.76
Model With Depth Refract'n	SWH	0.730	0.054	0.538	0.728	31.15	0.83
	Tm	0.919	0.590	0.782	0.705	17.55	0.77
Number of Data Points: 179; Mean Observed Values: SWH=2.345(m), Tm=5.236(s).							

Table 3.